-1-

MUON DEPOLARIZATION IN MATTER

Kenneth M. Crowe

Lawrence Berkeley Laboratory
University of California
Berkeley, California 94720

October 1973

INTRODUCTION

I see that my audience consists of specialists in the field, people who have heard talks on this subject, and a large fraction who (I assume) have not been exposed to this rapidly growing body of physics. Since I am addressing this talk to the last group, I apologize to the others, who know this material better than I, for repeating many well known and familiar facts.

My collaborators in this work include Jess Brewer from TRIUMF in Vancouver, Richard Johnson and Bruce Patterson of Lawrence Berkeley Laboratory, Alex Schenck of ETH in Zürich, Fred Gygax of SIN in Zürich, and Professor Don Fleming of the University of British Columbia in Vancouver.

In my talk I hope to cover the following topics, some rather briefly and others in detail: muons as probe; medium effects; experimental techniques; depolarization—fast and slow; and applications in chemistry, biology, and solids. Some topics will undoubtedly be omitted due to lack of time. Fortunately, people in the audience will have ample opportunity to fill in their special contributions; thus my discussions of these subjects will only be introductory.

MUONS AS PROBE

MASTER

Figure 1 is a summary of the important roles played by positive and negative muons over the years. Today I shall concentrate on μ^+ mesons in solid state and chemistry. Table I gives the numerical values of the constants that characterize the muon relative to other well-established probes. Note that the muon as a "light proton" has an even lighter companion, the positron;

in some examples, the muon's intermediate mass may give it a distinct advantage over the positron in complementing the results obtained with more conventional isotopes of hydrogen. Table II is intended to give the experimenters a quantitative feel for Larmor frequencies and periods associated with free muons and muonium, $(\mu^+ e^-)$ atoms, in typical magnetic fields used in these measurements.

MEDIUM EFFECTS

The slowing down of muons in various media has been discussed at great length. I will remind you only that the polarization of the muon is preserved for two related reasons: the energy-loss mechanism is Coulombic collisions with electrons in which the spin of the muon remains unchanged; and the whole timescale for slowing down, $\sim 10^{-11}$ sec, is such that only in enormous magnetic fields can the spin be turned.

The radiation damage at the position where the muon stops remains relatively little understood, especially at the very end of its range. We will discuss this in the last section.

Interactions of the muon with electrons at a few keV lead to the neutralization of a large fraction of the muons, with the formation of muonium atoms with excess kinetic energy. Reactions of muonium are similar to those of atomic hydrogen in the epithermal range. By studying the fraction of muonium atoms which form diamagnetic compounds during epithermal collisions, one expects to obtain reaction efficiencies which can be compared with "hot-atom chemistry" results for the other hydrogen isotopes. Some such results will be briefly discussed in Brewer's talk. The remaining muonium atoms thermalize then precess at the muonium frequency until they react to form either diamagnetic compounds or some other radical compounds. The latter type of compound is usually reactive and may later form a diamagnetic product. The entire chain

of reactions, it turns out, can be analysed; typical results will be shown in a later section.

SUMMARY OF EXPERIMENTAL TECHNIQUES

Such polarized muon beams as we are discussing are obtained by the decay of pions in flight in various geometries. The essentially 100% parity nonconservation in both pion decay and subsequent muon decay makes possible this observation of the motion of the spin of the muon.

Figure 2 shows the typical beam set-up. Counters M and E provide the start and stop timing signals which precisely record the lifetime of each muon. Figures 3 and 4 show the electronics, which I include only for those who are interested in the definition of the start-stop signals. Figure 4 also shows the PDP-15 computer set-up which is used to collect and digest the data.

As mentioned before, the muon comes to rest rapidly; so the arrival signal corresponds precisely to the start of muon precession. The muon decay occurs with an energy spectrum given by

$$N(E) = \left[\frac{\pi}{2}\right] \; X^2 \; \{(3-2X)_A + \xi\,(1-2X)_B \; \cos\,\phi\} \; dX \; d\Omega, \tag{1}$$

where $X = E/E_{max}$, ξ is the degree of polarization (≈ 1), and ϕ is the angle between the spin of the muon and the electron momentum.

The energy dependence of the spectrum and the asymmetry (B/A) are shown in Fig. 5. The lower curve shows that as one eliminates low-energy β particles, the average asymmetry can be increased from 1/3 to nearly 1.0. The asymmetry pattern can be observed directly as the muon spin precesses about an applied magnetic field, and the counting rate oscillates up and down corresponding to the muon pointing toward or away from the fixed detector. The rate then appears as follows:

$$N(t) = N_0 \; \exp(-t/\tau_\mu) \{1 + R(t)\,\xi\,\cos\,(\omega t + \phi)\} + BG, \tag{2}$$

where $R(t)$ is the depolarization effects, ω is the precession frequency due to

fields at the muon site, ϕ is the phase, and BG is the background ($\leq 5\%$).

Figure 6 shows the oscillations obtained in water at ~ 11 kG by collecting a large set of decays and combining them in an elapsed-time histogram; i.e., we take one muon at a time, record its lifetime to a fraction of a nanosecond, and bin $\sim 10^6$ such events to form this histogram. The top curve shows the first 100 nsec and the lower shows a similar interval 2 μsec later. From these data one can obtain a precise value for the muon magnetic moment. The story has been greatly oversimplified here; the figure only indicates the ability to extract precise frequencies from the analysis of such data.

DEPOLARIZATION

Variations of the apparent asymmetry from the maximum value given in Eq. 2 are described by the term R(t). Relaxation of the muon spin proceeds by two types of processes distinguished by their time scales: processes that take place too quickly to be observed directly with the technique described above, which has a resolution of the order $\leq 10^{-8}$ sec at best, are referred to as "fast"; processes that can be observed directly are called "slow." The slowest relaxation rates resolvable are in turn limited by our ability to follow the oscillations to large times as the muons decay; practically speaking, it would require prohibitively long runs to reliably measure relaxation times of > 10 μsec.

The obvious kinematic effects associated with partially polarized muons, finite angles in the detector system, etc. can be reduced typically to 20% reduction in polarization.

Muonium formation (discussed in the previous section) leads to a net reduction of the final asymmetry. Let us examine this mechanism in more detail. Figure 7 shows the hyperfine structure of the muonium atom as a function of external magnetic field. If the muon is located in a muonium atom, the energy levels follow this characteristic Breit-Rabi diagram; the relevant functions are:

Breit-Rabi hamiltonian

$$\mathcal{H} = a\,\vec{S}\cdot\vec{I} + g_e\mu_e^0\,HS_z - g_\mu\mu_\mu^0 HI_z$$

$$a = h\nu_0 = \frac{8\pi}{3}\,g_e\mu_0^e\,g_\mu\mu_0^\mu\psi^2(0)$$

For free 1-s muonium: $\psi(r) = \dfrac{1}{\sqrt{\pi a_0^3}}\ e^{-r/a_0}$

$(a_0 = \hbar^2/me^2)$

$$\Longrightarrow\quad a \approx \frac{16h}{3}\,\alpha^2 c\,R_\infty\,\frac{\mu_\mu^0}{\mu_e^0}\quad (g_e \approx g_\mu \approx 2)$$

$$\nu_0 = 4463.16\ \text{MHz}.$$

Solution: energy levels

$$E_{F = \frac{1}{2} \pm \frac{1}{2},\, M_F} = -\frac{a}{4} + g_\mu\mu_0^\mu\,HM_F \pm \frac{a}{2}\left[1 + 2\,M_F\,X + X^2\right]^{1/2}$$

$$\vec{F} = \vec{I} + \vec{S};\quad X = \frac{(g_e\mu_0^e + g_\mu\mu_0^\mu)H}{a} = \frac{H}{1580\ G}.$$

Spin eigenfunctions

$$\chi_{1,1} = \alpha_e\alpha_\mu$$

$$\chi_{1,0} = c\alpha_e\beta_\mu + S\beta_e\alpha_\mu$$

$$\chi_{1,-1} = \beta_e\beta_\mu$$

$$\chi_{0,0} = c\beta_e\alpha_\mu - S\alpha_e\beta_\mu$$

where

$$S_z\begin{pmatrix}\alpha_e\\\beta_e\end{pmatrix} = \pm\,\frac{1}{2}\begin{pmatrix}\alpha_e\\\beta_e\end{pmatrix}$$

$$I_z\begin{pmatrix}\alpha_\mu\\\beta_\mu\end{pmatrix} = \pm\,\frac{1}{2}\begin{pmatrix}\alpha_\mu\\\beta_\mu\end{pmatrix}$$

$$S = \frac{1}{\sqrt{2}}\left\{1 - \frac{X}{\sqrt{1+X^2}}\right\}^{1/2}$$

$$c = \frac{1}{\sqrt{2}}\left\{1 + \frac{X}{\sqrt{1+X^2}}\right\}^{1/2}$$

Half of the muonium atoms form in the ($F = 1$, $m = +1$) state and half in a superposition of ($F = 1$, $m = 0$) and ($F = 0$, $m = 0$). To a good approximation in weak fields, for the first half of the muonium, the muon spin precesses about the external field at a frequency determined by the magnetic moment of the electron (103 times faster than the free muon precession), while for the second half of the muonium the muon spin flips back and forth at the hyperfine frequency $\omega_0 = 2\pi\nu_0$. In stronger fields (comparable to the effective hyperfine field, 1588 G), the observable frequencies are the differences shown in Fig. 7, $\omega_{ij} = 2\pi\nu_{ij}$.

Figure 8 shows the behavior of the muon spin in a field of 100 gauss. The different times will be referred to later in the talk. One recognizes the hyperfine period $\tau = 0.24$ nsec, which in our detectors would not be resolved. Therefore, the polarization amplitude is immediately reduced to 50% and the remaining amplitude will oscillate about zero with the muonium frequency (Table II). If the field is above a few hundred gauss, this precession is also unresolved; and no asymmetry will appear. This is the so-called "proper" muonium depolarization mechanism.

In experimental situations (see Table III), the residual polarizations in various media fall into three groups: those with essentially 100% polarization remaining, those with $P_{res} \sim 1/2$, and a large group with a few percent residual polarization.

I will not go into the very interesting experiments in longitudinal fields and how one may understand the restoration of polarization, both at very low fields and at fields larger than the equivalent hyperfine field. Here there are a number of applications which have not yet been fully developed.

Let me turn to the "slow" phenomena. For an interesting example consider $CaSO_4 \cdot 2H_2O$, or gypsum. The NMR results for the proton spectrum of the protons in the water of crystallization of gypsum have been obtained and

are shown in Fig. 9. The interpretation by Pake, using a simple dipole-dipole mechanism where the field of one proton in the same water molecule produces a change in the field at the site of the other proton, can explain the pattern. There are two different locations for the water molecule in the crystal cell of gypsum. Pake showed (see Fig. 10) that rotation of the crystal produces a line separation and consequent equivalent relaxation of the NMR signal that arises from the beating of the individual lines. Table IV shows the line shape for muons if one assumes that the muon takes the place of a proton in one of these water molecules. The equivalent relaxation time T_2 can be calculated and compared with our experimental results. The results are remarkably consistent. This observation prompted us to look for beating between two of these "sites". Figure 11 shows the polarization as a function of time for one these orientations. Notice that the curve is calculated with the NMR results and the fit is excellent.

There are other examples of similar phenomena which will be mentioned later. The point here is that slow relaxation can be regarded as a result of varying internal fields, and hence the muon can act as a probe of these fields in some rather interesting examples. Note that in NMR, rapid relaxation of the signal causes the signal to disappear; whereas in the muon experiment, the faster the relaxation, the easier it is to observe, down to a fraction of a μsec.

APPLICATIONS

Time prevents me from dealing exhaustively with the increasing variety of applications of positive muons in disparate areas—in which, however, the muon seems to be particularily useful. In a review such as this I shall have to refer the audience to the extensive literature that has appeared and hope that, in the discussions, the details will come forth in questions.

Let me review the situation with respect to muons in gases by referring to the Hughes collaborations (e.g. see Ref. 1) and Mobley's thesis,[2] where they have established that traces of reactive materials in otherwise inert atmospheres cause the disappearance and/or spin relaxation of muonium. By studying the quenching of muonium resonance depolarization, they extract reaction cross sections for several interesting processes. Both thermal and hot-atom reactions can in principle be extracted in dilute gases; from the viewpoint of theoretical physical chemistry these data are of prime importance.

Reactions in dilute solutions have indicated the versatility of muon-tagged reactions in liquids. To be a bit more quantitative, we must first define the parameters involved:

[X] is the concentration of the reagent which is added to the solution;

τ is the mean lifetime of free muonium before chemical reaction;

k is the rate constant; and

$\tau = \dfrac{1}{k\,[X]}$ describes the relation between these quantities.

In principle one measures the asymmetries A_{Mu} and A_μ associated with muonium precession and "free" muon precession, respectively, as well as the decay times T_{Mu} and T_μ associated with each. For instance, a long-lived muonium signal would indicate a very long chemical lifetime τ; in that case, any free muon signal could be due only to hot-atom processes. In practice, no one has ever detected muonium precession directly in liquids. Brief muonium precession can be inferred, however, from variations of the apparent initial phase ϕ of the precession pattern described in Eq. 2. Figure 6 gives an indication of how this phase changes with chemical lifetime. Suppose the muonium reacts in a time $< < \tau_1$ (see Fig. 8). The spin will not have had any time to modulate or rotate; and the pattern will start precessing at an angle ϕ_0 determined by the geometry of the beam polarization, counter position,

curvature of the incoming and outgoing particles, and the precise definition of t_0, the origin of the time measurement.

Suppose now that the muonium lives for a substantial fraction of a hyperfine period. The average remaining muon polarization will be approximately 50%. If the lifetime is several HFS periods, the polarization will still be around 50%. However, if the chemical lifetime is long enough to survive a fraction of a muonium precession period, the slower average motion (see Fig. 8) will also have rotated. If the field is sufficiently high, the muonium rotation is comparable to the hyperfine oscillation, so that this regime will be limited to low fields. When this model is described more rigorously, these expectations are indeed realized. Figure 12 shows a case in which iodine (I_2) has been dissolved in methanol (CH_3OH). Note the "shoulder" of the asymmetry, which occurs when the lifetime, $\tau = 1/k[I_2]$, is between the HFS period and the Mu period. The curve is a best fit to the data, based on the theory worked out by Ivanter and Smilga, commonly called the "proper muonium mechanism" for fast depolarization. Brewer et al. expanded the theory to include situations involving more than one strongly depolarization influence, i.e. muonium and molecular radicals.

Figure 13 illustrates how muons may branch to the various channels. The figure shows most of the possible different paths to "free" muon precession; the above-mentioned paper gives the formal analysis in detail. Fortunately, Brewer, Gygax, and Fleming are in the audience today; so I urge you to direct questions to them on these subjects.

Let us not, however, leave this subject without a few examples of how the data and theory agree. As mentioned, Fig. 12 gives the results for I_2 dissolved in methanol. Figure 14 shows the situation for bromine in benzene. The dotted curve which ignores the radical-formation branch does not come near to fitting the results. However, adding these channels gives excellent agreement for the

residual polarization and improves the phase fit considerably. Figure 15 shows a similar result for H_2O_2; the fit is extremely satisfying. Figure 16 shows the efficacy of the nitrate ion in scavenging muonium, while Fig. 17 similarily indicates the perchlorate ion reacting with muonium.

To summarize these phenomena, Table V lists the qualitative results of the best fits to the data with and without radical formation, giving the relevant solvents, reagents, fields, asymmetries, and quality of fit. I include Tables VI and VII mainly to give the readers of the Proceedings a chance to see the quantitative results and the comparison with the corresponding atomic hydrogen results.

At this point the discussion becomes rather specific to each reaction— the results being explainable simply in terms of the extra velocity the muonium has (compared with hydrogen) due to its lighter mass; these results show that the tunneling or barrier penetration can be entirely different for the muonium atom.

Brewer has agreed to supplement this talk with some remarks concerning the hot-atom reactions and comparisons that again show both similarities to and variations from the corresponding reactions of heavier isotopes of hydrogen.

Let me diverge slightly to mention how extensive the prospects may be for these studies. As you know, biologists are quite concerned with the migration of water in complex systems. Radical formation may be a significant clue to cancer development and metastasis. One should carefully consider how this new tool may be introduced to problems of living cells.

Let me turn now to earlier studies on concentrated solutions of paramagnetic ions. This subject shows another direction in which muons may be utilized.

Earlier, I mentioned the influence of adjacent protons on each others' NMR spectra in solid $CaSO_4 \cdot 2H_2O$. In a natural extension of these studies,

the depolarizing effects of paramagnetic ions in aqueous solutions have shown that muons do indeed replace protons in water molecules and subsequently find themselves depolarized in a way entirely analogous to protons.

Figure 18 illustrates the concentration dependence of the transverse relaxation time for protons in water for solutions of various paramagnetic ions. Bloembergen, Purcell, and Pound (BPP)[3] have discussed these processes in a classic paper; their theory has explained many important quantitative results in this field. If one scales the formulae appropriately with the higher magnetic moment associated with the muon, there is a remarkably good fit for a number of cases.

Figure 19a shows transverse muon relaxation times in solutions; at low concentrations the data agree precisely with the scaled-down proton results. Note that as the concentration becomes higher, the points deviate from the curve. This puzzling deviation from the BPP theory, which to our knowledge has never been observed with conventional proton NMR, can be explained by a relaxing of the electron spin of the manganese ion due to adjacent manganese ions, which has the effect of quenching the process that relaxes the muon's spin. Figure 19b shows the ESR data on the electron spin correlation time, measured independently by Hinckley and Morgan.[4] When this process is included in the BPP theory, there is a drastic improvement to the fit, as shown in Fig. 20a.

Here again the muon has extended the range of measurements of paramagnetic relaxation well beyond the conventional NMR results, uncovered an interesting 3-body quenching mechanism, and left open the possibility of extensions to similar concentrated solutions where NMR data will probably be unavailable due to the very broad line width.

The second half, Fig. 20b, shows the temperature dependence in the same solution. Here the agreement is rather poor. Clearly many of the assumptions

made in this simplified model need to be tested. The field dependence, con-
centration dependence, and temperature dependence of relaxation by this ion
and others, as well as complementary measurements by conventional techni-
ques, will be necessary before one can hope to understand quantitatively all
the phenomena associated with these data.

The relaxation of muons in solids—for example, metals, insulators,
superconductors, semiconductors, magnetic materials, and alloys—opens up
an enormous number of possibilities. Although we have dabbled in these sub-
jects, I shall mention only a few salient results which may suggest applica-
tions to the specialists.

Gurevich et al. [5] have shown that the relaxation of muons in copper is due
to dipole-dipole interactions with the magnetic nuclei, and can be related to the
diffusion of the muons through the lattice.

We find that most insulators have relaxation phenomena that vary due to
the presence or absence of ferromagnetic impurities, paramagnetic impurities,
and other more intrinsic properties of the materials.

The muon in superconducting lead verifies the Meissner effect. When the
temperature is decreased below the critical point in an external field, the lack
of precession of the muon verifies that there really are no internal fields.
Type II superconductors have not been studied by us, although they clearly
have interesting possibilities. Kossler will discuss his recent data on nickel
and iron in a later talk.

Let me finish by describing a recent result arising from studies of muons
in semiconductors. If we recall Fig. 7, we expect that the frequencies present
in the hyperfine spectrum will include the various allowed differences between
the energy levels shown. We label the levels 1, 2, 3, and 4 in order of de-
creasing energy. For muons stopping in quartz, Gurevich et al. [6] showed
that there was a beating of the two muonium precession frequencies, ω_{12} vs ω_{23},

whose quadratic field dependence could be analyzed to extract ω_0. They found ω_0 (quartz) approximately the same as ω_0 (vacuum). On the other hand, in germanium they found ω_0 (Ge)/ω_0 (vac) = 0.58(4).

We have made similar measurements in silicon. Figure 21 shows a comparison between Fourier transform data for quartz and silicon in the same field. The two highest frequencies correspond to ω_{12} and ω_{23} of muonium. Their separation is proportional to $1/\omega_0$ and is clearly larger for silicon. Analysis yields ω_0 (Si)/ω_0 (vac) = 0.444(20).

These results have been satisfactorily interpreted by Wang and Kittel in a recent paper. [7] Their model has muonium trapped in an interstitial site that is large enough to contain the orbital electron in the ground state. Roughly speaking, the binding potential is cut off at large radius due to screening by the valance band electrons of the surrounding atoms of silicon. By using other data, they can explain the size of the change in the hyperfine frequency as well as the difference between Ge and Si in terms of the increase in the size of the muonium atom caused by the neighboring atoms of the crystal. This model, the deep-donor for muonium in semiconductors, seems to be in accord with observations. Wang and Kittel observe that "it is not possible at present to compare these values with those for atomic hydrogen---since the presence of atomic hydrogen has never actually been detected---." Further, "we know more about muonium in Ge and Si than about H or H_2 in just these crystals on which rests most of modern solid state electronics technology."

In Fig. 21 one can see that there are other Fourier components in addition to the two muonium lines. One expects that the free muon will appear in this figure near zero. However, there are two "stronger" lines at intermediate frequencies, which we have labelled "anomalous precession." We have varied the field in an attempt to follow these lines; Figure 22 shows the data we have

accumulated to date. The two sets of points are associated with different crystal orientations, i.e. [111] and [100], along the field axis. The data are taken with the sample at liquid N_2 temperature, for mildly p-type silicon. Both anomalous precession and muonium precession have a lifetime on the order of 300 nsec. Neither of these signals has been detected in n-type Si at 77°K or in any silicon sample at room temperature.

The anomalous frequencies are much higher than the free muon precession frequencies in weak magnetic fields. The muon must therefore be coupled to a particle or system with a larger magnetic moment than its own, as in muonium where it is coupled to an electron by the contact interaction. The field dependence of the data can in fact be fitted to frequencies ν_{12} and ν_{34} of a modified Breit-Rabi formula (see Fig. 7) if the different crystal orienta-tions are treated as separate cases. However, it is necessary to allow both the hyperfine coupling strength and the g-factor of the electron to vary in order to obtain a fit. For the case of the [111] crystal axis parallel to the field, the best value for ν_0/ν_0 (vac) is 0.0198(2); for [100] parallel to the field, the best value is ν_0/ν_0 (vac) = 0.0205(3). In both cases, the best value for g_e is 13 ± 3. Clearly, the spin g-factor of an electron cannot be much different from 2, nor can a pure contact interaction be anisotropic; this modified Breit-Rabi description is meant only as a phenomenological characterization of the data.

These results can be interpreted in terms of several physical models. Perhaps the simplest is shallow-donor muonium. Here the electron wave-function is spread over many lattice sites, whereas the entire deep-donor muonium atom fits into one interstitial site. An s-state cannot produce the observed behavior, due to the relatively invariable spin g-factor of the elec-tron. However, in the 2p state the orbital g-factor can be large and anisotropic:

the electron wavefunction for a shallow donor must be a superposition
of conduction band states, which may have small, anisotropic effective masses.
A possible objection to this model is the requirement of a minimum lifetime of
~ 300 nsec for the 2p excited state. Hindrance of the normally fast radiative
E1 transition $2p \rightarrow 1s$ can be explained by the small overlap between electron
wavefunctions in the shallow-donor 2p state and the deep-donor 1s state.

A second physical model is suggested by the large variety of ESR centers
which have been observed in radiation-damaged silicon. [8] The muon may
create a paramagnetic lattice defect (e. g. , a broken bond) at the end of its
range, combining with it to form a muon-defect bound state. Such a center
can also be described by a modified Breit-Rabi hamiltonian.

The possibility that the anomalous precession is due to formation of a
bound state of a muon with an impurity atom is considered remote.

However, in stopping, the muon must generate a high density of free elec-
trons and holes, with which it may subsequently combine. If we regard the
μ^+ as a positive impurity ion in an interstitial position, observations of im-
purity-exciton bound states in silicon provide a precedent for two models in-
volving excitons. The first model is the neutral muonium-exciton molecule
$(\mu^+ e^- e^- h^+)$, in which the two electrons are assumed to have paired spins, in
analogy with ground-state H_2. The μ^+ is thus coupled to the hole by a dipole-
dipole interaction. Orientational effects are predicted by this model if the
molecule is "pinned" by being wedged into an oblong interstitial site in the
unit cell. A second model of this type is the ionized muonium-exciton molecule
$(\mu^+ e^- h^+)$, in which all three particles are coupled via contact interactions.
These models draw support from the fact that measured free exciton lifetimes
in silicon at 80°K are about 400 nsec. [9]

None of the above physical models for anomalous muon precession can
be eliminated on the basis of existing data; however, we feel that shallow-
donor 2p muonium is the most probable explanation.

FOOTNOTE AND REFERENCES

*Work performed under the auspices of the U. S. Atomic Energy Commission.

1. R. M. Mobley, J. J. Amato, V. W. Hughes, J. E. Rothberg, and
P. A. Thompson, J. Chem. Phys. 47, 3074 (1967).

2. R. M. Mobley, "Interactions of Muonium with Atoms and Molecules",
Ph. D. thesis, Yale University, 1967.

3. N. Bloembergen, E. M. Purcell and R. V. Pound, Phys. Rev. 73, 679
(1948).

4. C. C. Hinckley and L. O. Morgan, J. Chem. Phys. 44, 898 (1966).

5. L. I. Gurevich et al.,   Phys. Letters 40A, 143 (1972).

6. I. I. Gurevich et al., Soviet Phys. JETP 33, 253 (1971).

7. S-Y. Wang and C. Kittel, Phys. Rev. B7, 713 (1973).

8. G. Lancaster, ESR in Semiconductors (Plenum Press, N. Y., 1967).

9. V. S. Vavilov, É. L. Nolle, Fis. Tekh. Poluprov. 2, 742 (1968);
Sov. Phys. —Semicond. 2, 616 (1968).

Table I. Properties of the muon

Spin = $\frac{1}{2}$

Mass: M_μ = 105 Mev = 206.76 $M_{electron}$ = 0.112 M_{proton}

Magnetic moment: $\mu_\mu = g_\mu \dfrac{e\hbar}{2M_\mu c}$ = 3.183347 μ_P

$\qquad\qquad\qquad\quad$ = 2.8×10^{-17} MeV/gauss

Lifetime: τ_μ = 2.1983×10^{-6} sec

Larmor frequency = ν_μ = 13.5 kHz/gauss

Muonium Larmor frequency: ν_{Mu} = 1.4 MHz/gauss

Muonium hyperfine frequency: $\Delta\nu_0$ = 4463 MHz

Table II. Precession frequencies and periods in various fields

B	10G	100G	1kG	10kG	100kG
ν_μ (MHz)	0.135	1.35	13.5	135	1350
T_μ (nsec)	7400	740	74	7.4	0.74
ν_{Mu} (MHz)	14	140	1400	too fast to see	
T_{Mu} (nsec)	70	7	0.7	too fast to see	

Table III. Asymmetry coefficients for positive muons

Medium	Asymmetry coefficient	Error	Medium	Asymmetry coefficient	Error
Graphite	0.229	0.008	HCl pH = 1.2	0.158	0.011
Graphite	0.24	0.04	Polyethylene	0.146	0.012
Soot	0.253	0.021	Polyethylene	0.20	0.03
Bromine	0.34	0.06	Polystyrene	0.070	0.010
Al	0.209	0.010			
Diamond	0.045	0.008	Polystyrene + 2% p-terphenyl	0.06	0.04
Diamond Be	0.222	0.012	Propane	0.170	0.020
Diamond Li	0.201	0.014	Benzene	0.046	0.012
Diamond Mg	0.254	0.013			
Diamond Mg	0.20	0.05	Phenylcyclo- hexane	0.084	0.011
Diamond Si	0.253	0.012	Chloroform	0.184	0.015
Diamond Si	0.21	0.06	P	0.025	0.017
Diamond Cu	0.24	0.02	S	0.014	0.011
SiC	0.213	0.011			
B_4C	0.23	0.02	CsI	0.031	0.013
Al_2O_3	0.022	0.009	NaCl	0.041	0.009
			MgF_2	0.136	0.009
Fused quartz (SiO_2)	0.038	0.009	MgO	0.079	0.012
			Emulsion	0.087	0.009
Crystalline quartz	0.01	0.02	Emulsion	0.13	0.02
			AgBr	0.02	0.02
Water pH = 6.5	0.141	0.011	Gelatine	0.12	0.03
Distilled water	0.14	0.03	CCl_4 (liquid)	0.26	0.05
			Methyl alcohol	0.16	0.05
NaOH = 12	0.131	0.012			

Table IV. Comparison between relaxation measurements and calculations for different orientations of the gypsum crystal. The crystal axes are given in the Onorato convention: (100) = x, (010) = y, $z \perp (x, y)$. The measured T_2^* are independent of magnetic field strength.
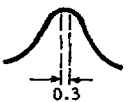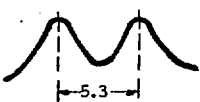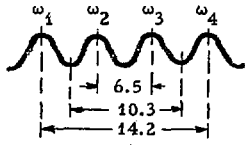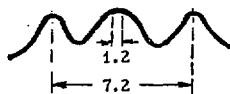
Position	Crystal orientation	Muon - NMR spectrum [scale = gauss]	Calculated T_2^* from NMR spectrum	Measured T_2^* (μsec)
1	$\vec{H}, z = 90°$ $\vec{H}, x = 94°$ $\vec{H}, y = 57.5°$	5 G	5.6	5.50 $\pm$.50
2	$\vec{H}, z = 90°$ $\vec{H}, x = 146°$ $\vec{H}, y = 62.5°$	1.8	9.0	10.5 1.00
3	$\vec{H}, z = 90°$ $\vec{H}, x = 176°$ $\vec{H}, y = 32.5°$	0.3	10.50	10.50 1.00
4	$\vec{H}, z = 0$ $\vec{H}, x = 90°$ $\vec{H}, y = 90°$	5.3	5.3	4.80 $\pm$.30
5	$\vec{H}, z = 40°$ $\vec{H}, x = 142°$ $\vec{H}, y = 111°$	ω_1 ω_2 ω_3 ω_4 6.5 10.3 14.2	2.9	3.09 $\pm$.20
6	$\vec{H}, z = 24°$ $\vec{H}, x = 90°$ $\vec{H}, y = 66°$	1.2 7.2	5.60	5.50 $\pm$.40
Polycrystal, powder			5.3	5.30 $\pm$.20
Polycrystal, anhydrous			---	60. $\pm$20.

Table V
BEST FITS TO GENERAL MECHANISM (WITH RADICALS)

REAGENT	SOLVENT	FIELD (gauss)	$\frac{\omega_r}{\omega_o}$ [a]	A_o	ϕ_o (deg)	h	RATE CONSTANTS × 10^{-10}				$\frac{\chi^2}{\text{deg. fr.}}$
							k_{mxd}	k_{rxd}	(Z)	k_{mzr}	
H_2O_2	H_2O	100	$.083^b$	.26	10.82	.59	.24	.14	(X)	.83	~ 1
				±.01	±.5	±.01	±.1	±.05		±.2	
HNO_3	H_2O	100	$.125^c$	.277	15.76	.546	3.25	.111	(X)	13.0	~ 1.5
			±.05	±.01	±.75	±.02	±2.0	±.05		±7.0	
Br_2	C_6H_6	200	$.095^d$	.271	38	.134	9.5	.36	(S)	.125	~ 2
				±.005	±1	±.01	± 2	± .1		± .05	
I_2	C_6H_6	200	$.095^d$	.272	35	.128	5.8	.2	(S)	.054	~ 1
				±.02	±2	±.06	± 2	± .1		± .03	

Rate constants in liters/mole-sec.

Errors are approximate. Differences in ϕ_o are due to changes in counter geometry between series of runs.

[a] Values for ω_r of specified radicals obtained by multiplying μ_μ/μ_p = 3.18 into measured value of hyperfine frequency for hydrogen version of radical (from Landolt & Bornstein).

[b] Radical involved presumed to be MuO·   [c] Radical species not identified.

[d] Radical involved presumed to be C_6H_6Mu·

XBL 726-1081

Table VI

BEST FITS TO "PROPER" MUONIUM MECHANISM

REAGENT	SOLVENT	FIELD (gauss)	A_o	ϕ_o (degrees)	h	$k_{mxd} \times 10^{-10}$ (liters/mole-sec)	$\dfrac{\chi^2}{\text{deg. fr.}}$	MECHANISM CORRECT?
I_2	CH_3OH	103	.24 ± .01	15.5 ± 1.0	.54 ± .02	16.7 ± 2.0	∿2	yes
"	"	1000	.27 ± .02	105 ± 2[a]	.52 ± .02	11.4 ± 2.0	∿3.5	yes
"	"	4500	.27 ± .02	—	.54 ± .02	13.4 ± 2.0		yes
$FeCl_3$	H_2O	4500	.31 ± .02	—	.51 ± .02	2.1 ± 0.2	∿1	?
$Fe(ClO_4)_3$	H_2O	4500	.30 ± .02	—	.55 ± .02	1.7 ± 0.2	∿6	no
"	"	100	.275[b]	15.5[b]	.55[b]	0.24	∿100	no
$HClO_4$	H_2O	4400	.275[b]	—	.54 ± .01	0.12	∿2	?
HNO_3	H_2O	4500	.30 ± .01	—	.54 ± .01	0.64	∿1.5	no
"	"	100	.275[b]	16.2 ± 4.0	.55[b]	0.62	∿11	no
H_2O_2	H_2O	100	.26 ± .02	11.4 ± 1.2	.58 ± .02	0.45	∿3	no

[a] $t = 0$ not defined; ϕ_o therefore arbitrary.   [b] Parameter held constant; not fitted.

Errors quoted are approximate. χ^2/degree of freedom is apt to have been overestimated, due to probable undetected systematic uncertainties.

XBL 726-1080

Table VII
SURVEY OF SOLVENTS

SOLVENT NAME	FORMULA	A	ϕ (deg)	h	COMMENT
WATER	H_2O	.15 ± .01	15 ± 4	.55 ± .01	no "cold" reaction
METHANOL	CH_3OH	.13 ± .01	13 ± 3	.53 ± .01	"
BENZENE[a]	C_6H_6	.036±.005	33 ± 3	.13 ± .01	"cold" reaction to radical only
CARBON TETRACHLORIDE	CCl_4	.272±.010	14 ± 3	$\sim 1.0^b$	density may be a factor
GLYCEROL	$C_3H_8O_3$	.179±.010	13.5±3	$\sim.65^b$	"
HEXYNE	C_6H_{10}	.103±.010	6.5 ±4	$\sim.4^b$	very unsaturated
HEXENE	C_6H_{12}	.119±.010	9 ± 3	$\sim.45^b$	unsaturated
HEXANE	C_6H_{14}	.145±.010	10 ± 3	$\sim.55^b$	saturated
CYCLOHEXANE	C_6H_{12}	.160±.010	8 ± 3	$\sim.6^b$	"

Errors are approximate.

Magnetic field is 100 gauss unless otherwise specified.

[a] Magnetic field = 200 gauss.

[b] assuming no "cold" reaction.

XBL 726-1082

FIGURE CAPTIONS

Fig. 1. Various experiments in progress which utilize the muon as a probe of matter.

Fig. 2. Typical beam set-up. Top and side views of stopping target, counter arrangement, and magnet coils. (Not to scale)

Fig. 3. Fast logic for muon experiments.

Fig. 4. Block diagram of logic network.

Fig. 5. Muon decay spectrum. Top curve: unpolarized spectrum. Bottom curve: asymmetry contribution.

Fig. 6. Two short sections of the data, for which there were 3.4 million analyzed events. The smooth curve is the maximum-likelihood fit.

Fig. 7. Hyperfine structure of muonium as a function of external magnetic field.

Fig. 8. Evolution of muon polarization in free muonium in 100-G transverse field. P_X^μ = projection of μ^+ polarization along original polarization direction.

Fig. 9. NMR spectra of protons in the water of crystallization of gypsum for different crystal orientations.

Fig. 10. NMR spectrum analyzed using a simple dipole-dipole model for the two water molecules.

Fig. 11. The observed asymmetry, AF(t), for the gypsum crystal having two NMR lines. Asymmetry is calculated for 0.5-µsec intervals vs. muon lifetime. Solid curve shows the theoretical AF(t).

Fig. 12. Results for iodine dissolved in methanol.

Fig. 13. Flow chart of depolarization mechanism.

Fig. 14. Bromine dissolved in benzene at 200 gauss: fit including radical formation.

Fig. 15. Results for H_2O_2.

Fig. 16. HNO_3 at 100 gauss: fit including radical formation.

Fig. 17. $HClO_4$ at 4400 gauss: fit assuming proper muonium mechanism.

Fig. 18. Concentration dependence for transverse relaxation time for protons in water for solutions of various paramagnetic ions.

Fig. 19(a). Transverse muon relaxation times in $MnCl_2$ solutions. The dashed lines represent the spin-exchange and dipole-dipole terms. The solid line is the combined result. (b). Plot of τ_s^* vs. Mn^{2+} concentration at 295°K. Solid line was obtained from Ref. 4.

Fig. 20(a). Plot of $1/T_2p$ vs. Mn^{2+} concentration. The solid curve is obtained by combining NMR and ESR results. The dashed curves show separately the contributions from spin-exchange and dipole-dipole interactions.

(b). Plot of $1/T_2p$ vs. temperature. Dotted curve is the fit obtained without modifications. Solid curves result from our analysis at 4.5 and 11 kG. Dashed curves represent the spin-exchange and dipole-dipole contributions of our analysis separately to 11 kG.

Fig. 21. Frequency spectra of muons in fused quartz at room temperature and in p-type silicon at 77°K. In both cases the applied field is 100 gauss. The vertical axis is the square of the Fourier amplitude, in arbitrary but consistent units. In the lower graph the vertical scale is expanded by a factor of 10 to the right of the dashed line. The prominent peaks (from left to right) are: the free muon precession signal at 1.36 MHz; a characteristic background signal at 19.2 MHz, due to rf structure in the cyclotron beam; the two anomalous frequencies at 43.6±2.9 MHz (silicon only); and the two 1s muonium peaks centered about 139 MHz. The wider splitting of the two 1s muonium lines in silicon is due to the weaker hyper-fine coupling. These spectra were produced by Fourier analyzing the first

750 nsec of the experimental histograms. For comparison, the muon asymmetries obtained by maximum-likelihood fits to the first 5 μsec of data were $3.81 \pm 0.35\%$ for quartz and $5.05 \pm 0.63\%$ for p-type Si at $77°$ K.

Fig. 22. Dependence of anomalous frequencies in silicon upon field strength and crystal orientation. Round points and solid lines are data and best fit for (111) crystal axis along the field; triangular points and dashed lines are data and best fit for (100) axis along the field. Free muon, 1s muonium, and cyclotron background signals are not shown. A number of peaks appear in the spectra in addition to the fitted "proper" anomalous frequencies; these are unexplained. They are indicated by square points (for prominent peaks) and horizontal bars (for weak or questionable peaks). The higher of the "proper" anomalous frequencies is missing at several fields. This is because the spectra showed no statistically significant peaks at those positions.

APPLIED MUON PHYSICS
THE MUON: AN IDEAL ELECTROMAGNETIC PROBE.
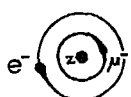
μ^- THE HEAVY ELECTRON μ^+ THE LIGHT PROTON

ATOMIC PHYSICS

MUONIC ATOMS

X-RAYS & ATOMIC STRUCTURE
μ^- PRECESSION
RELATIVISTIC EFFECTS
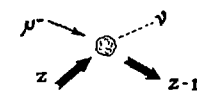
MUONIUM

QED TEST { Mu HYPERFINE
MUON MOMENT
MUON "G-2"

NUCLEAR PHYSICS

μ^- CAPTURE
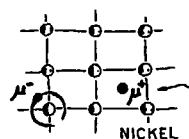
WEAK INTERACTIONS IN NUCLEI

NUCLEAR STRUCTURE FROM
DEEXCITATION γ'S

SOLID STATE PHYSICS

FERROMAGNETS

PROBE LOCAL MAGNETIC
FIELD NEAR NUCLEUS

FERROMAGNETS

PROBE INTERSTITIAL
LOCAL MAGNETIC FIELD
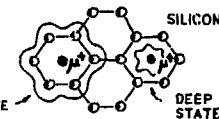
NICKEL

SEMICONDUCTORS
STUDY IMPURITY STATES

SILICON
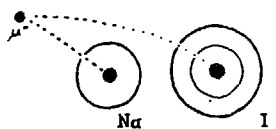
SHALLOW STATE

DEEP STATE

CHEMISTRY

MUONIC ATOMS

Na   I

MUONIUM VS HYDROGEN ATOMS

EG: $Mu + I_2 \rightarrow MuI + I$

COMPARE WITH: $H + I_2 \rightarrow HI + I$

Fig. 1.

Fig. 2.

XBL 735-2916

FROM COUNTERS   TO SLOW LOGIC
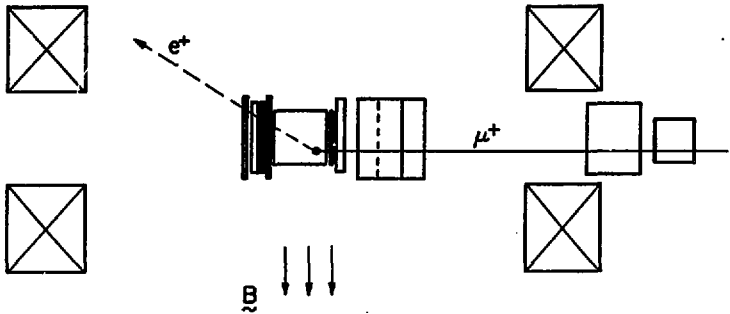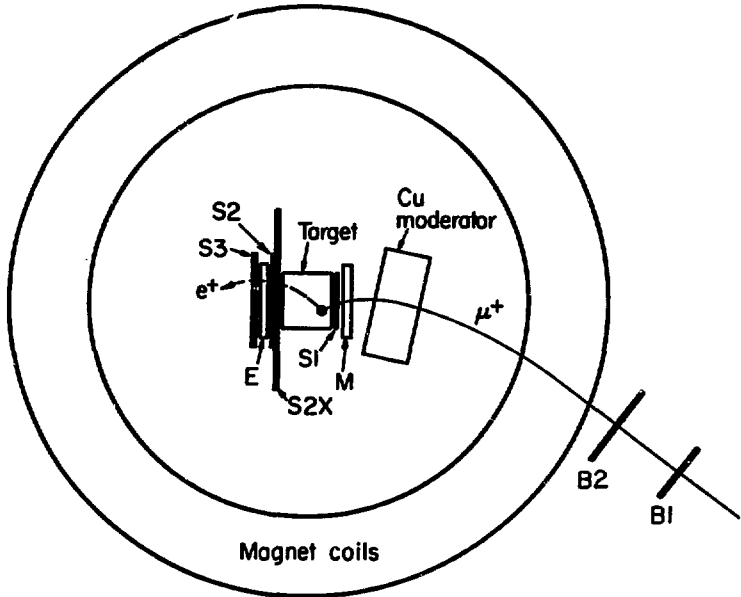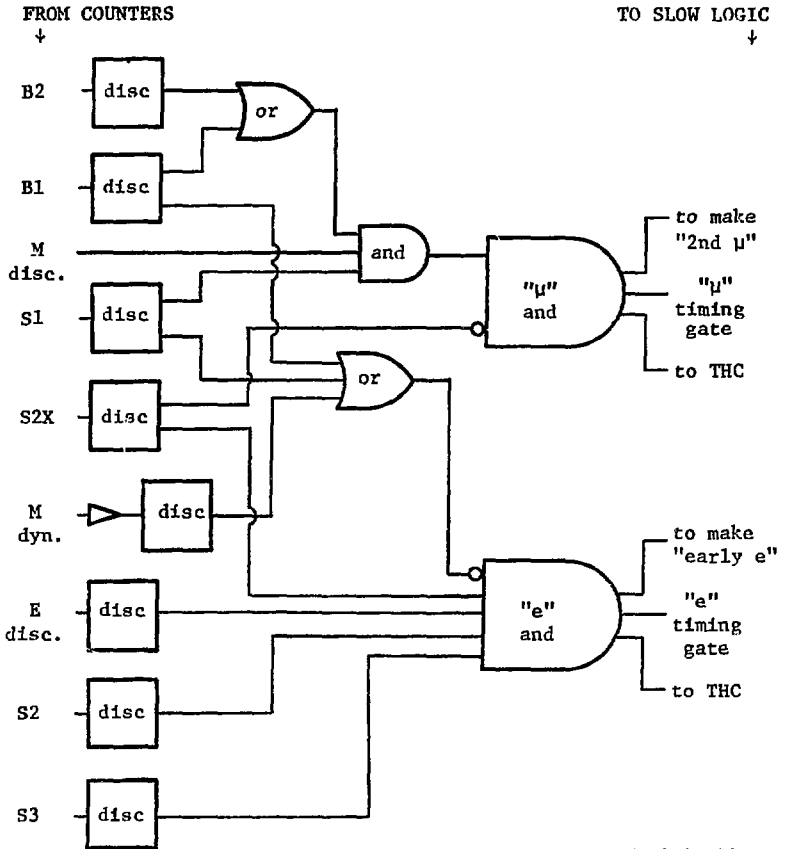
Fig. 3.   XBL 726-1088
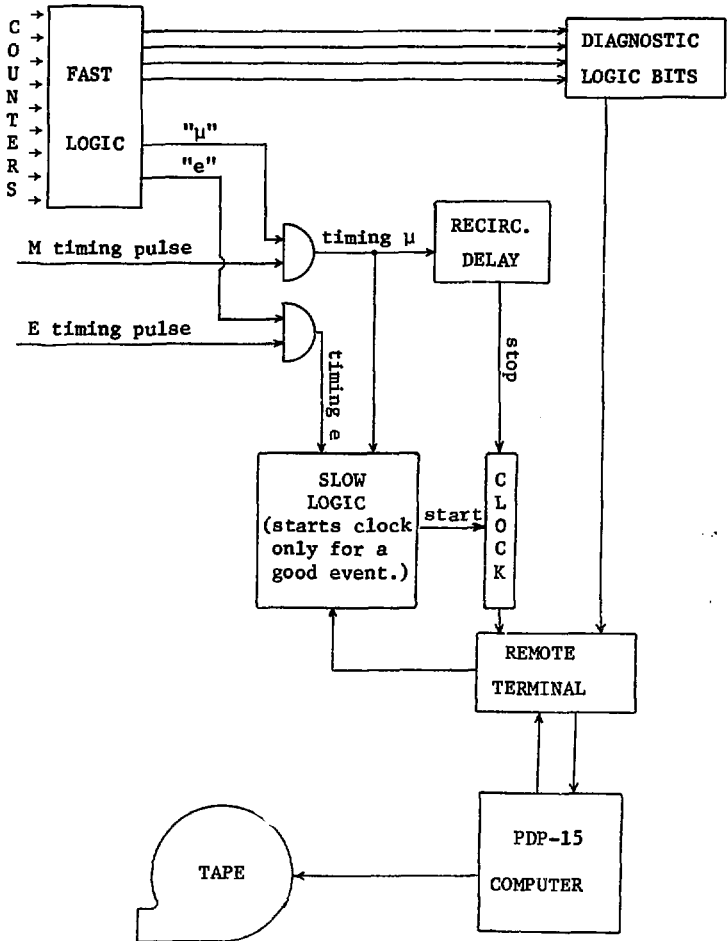
Fig. 4.   XBL 726-1094
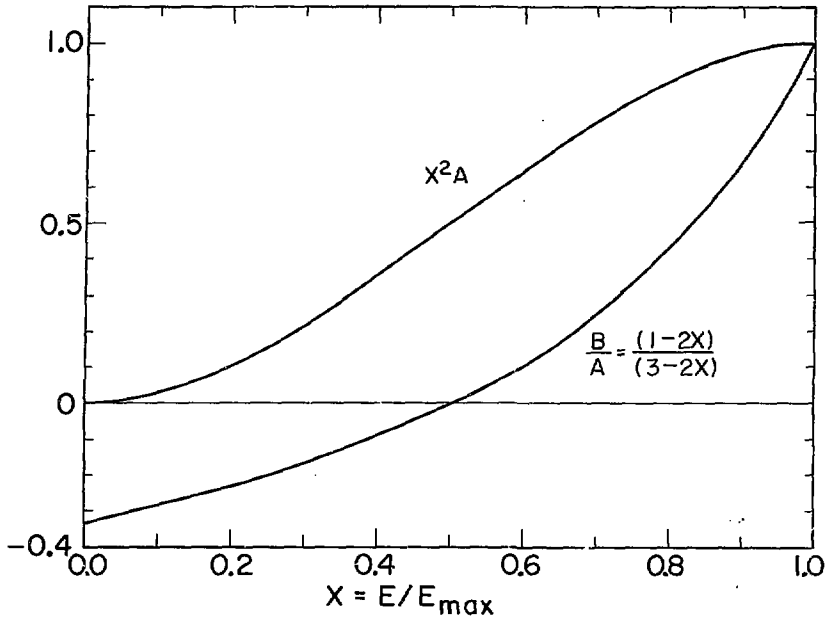
XBL739-4066

Fig. 5.
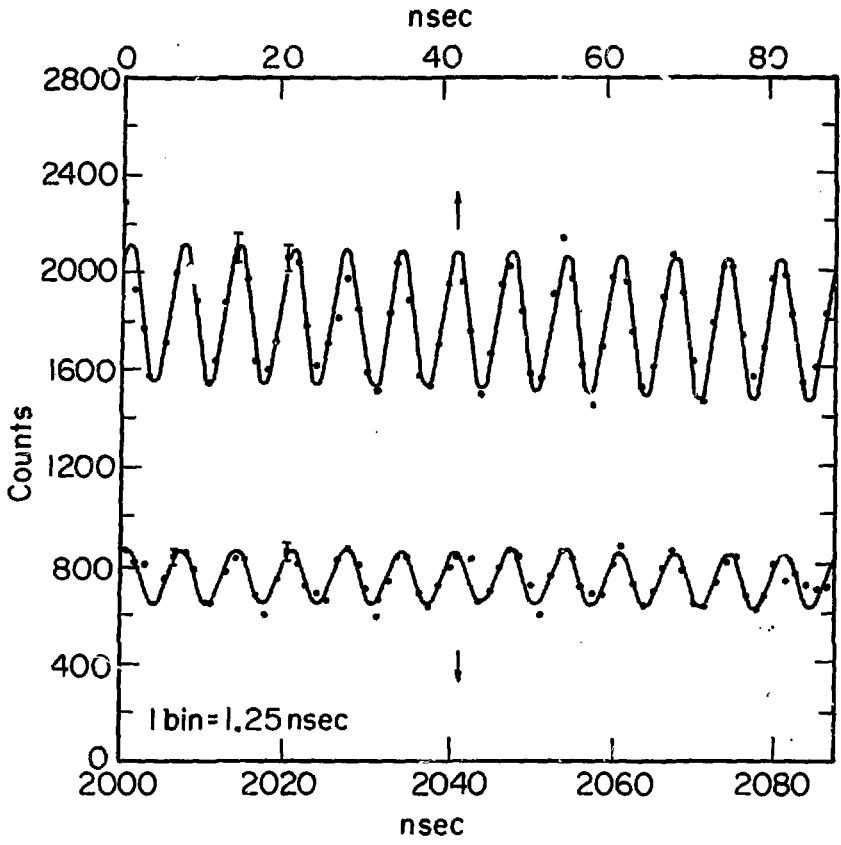
XBL 739-4065

Fig. 6.
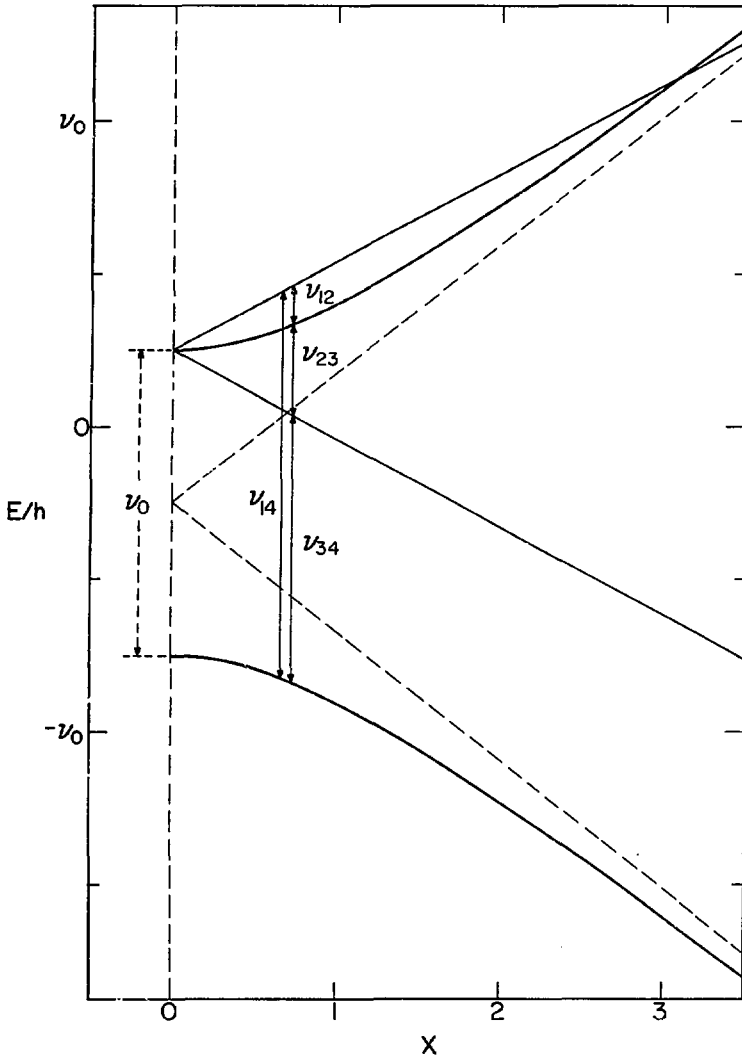
Fig. 7.   XBL733-2502
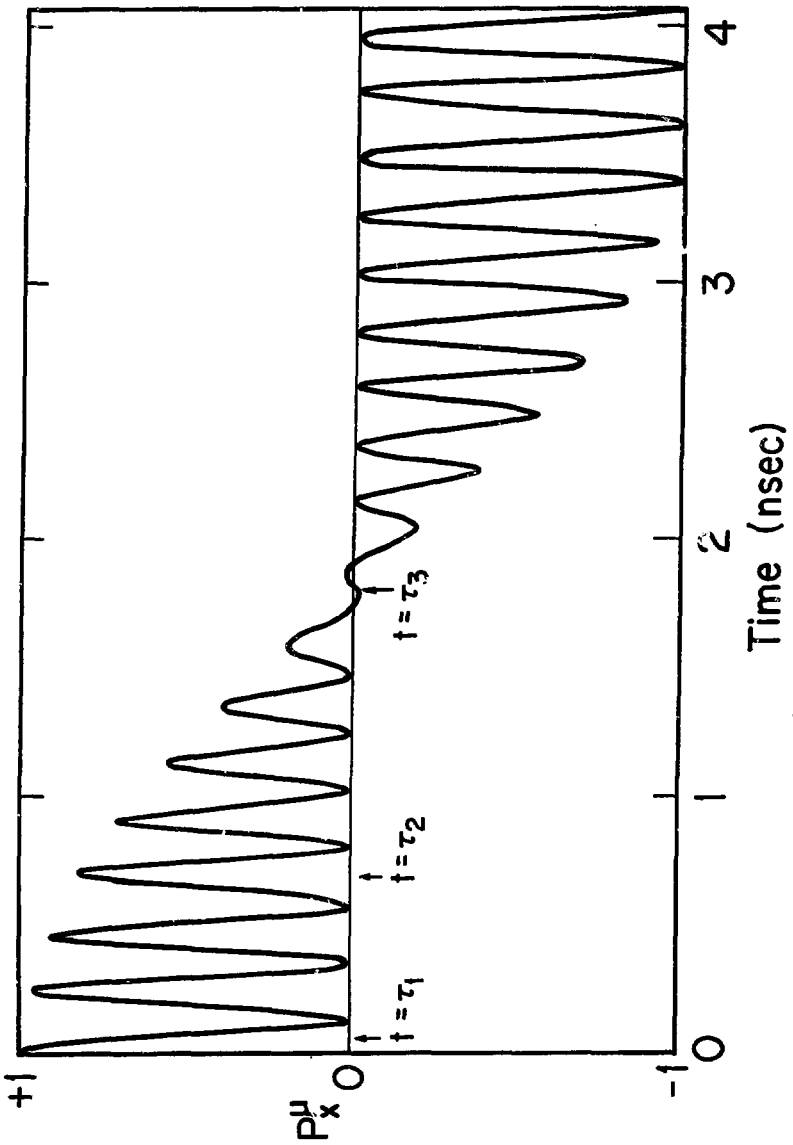
Fig. 8
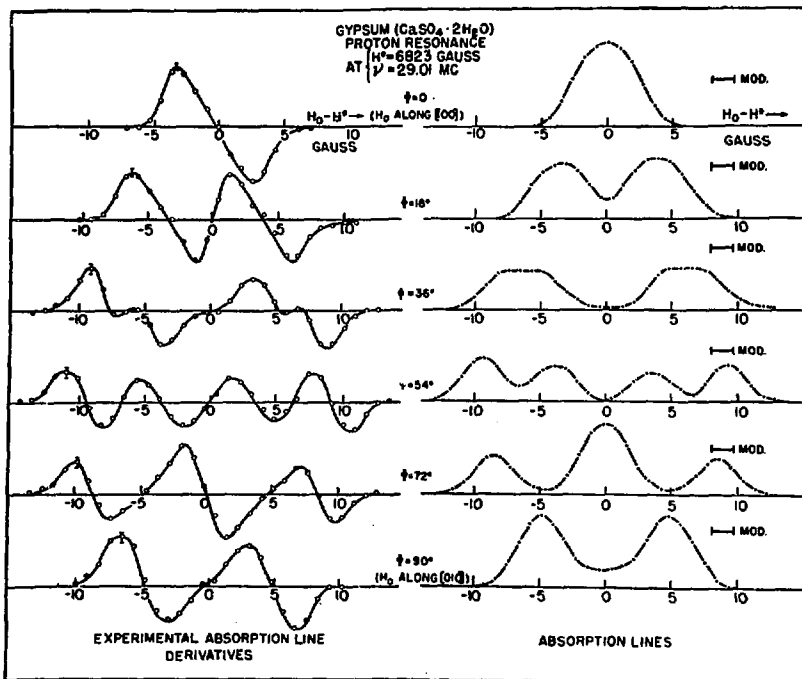
XBL7210-4190

Fig. 9.
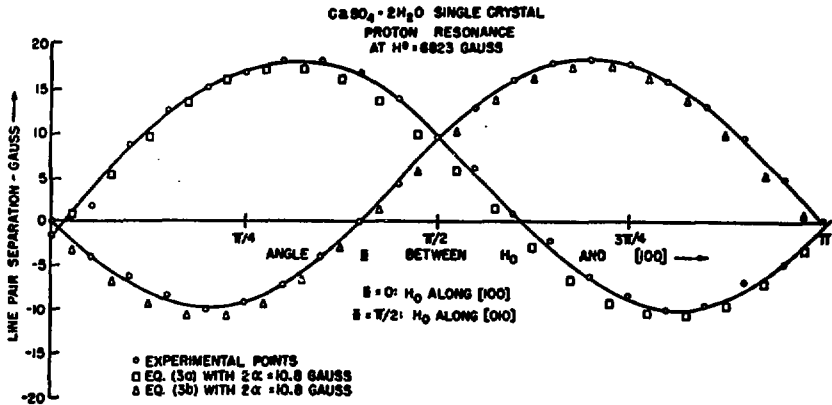
XBL 708-1705

Fig. 10.

XBL7011-4115
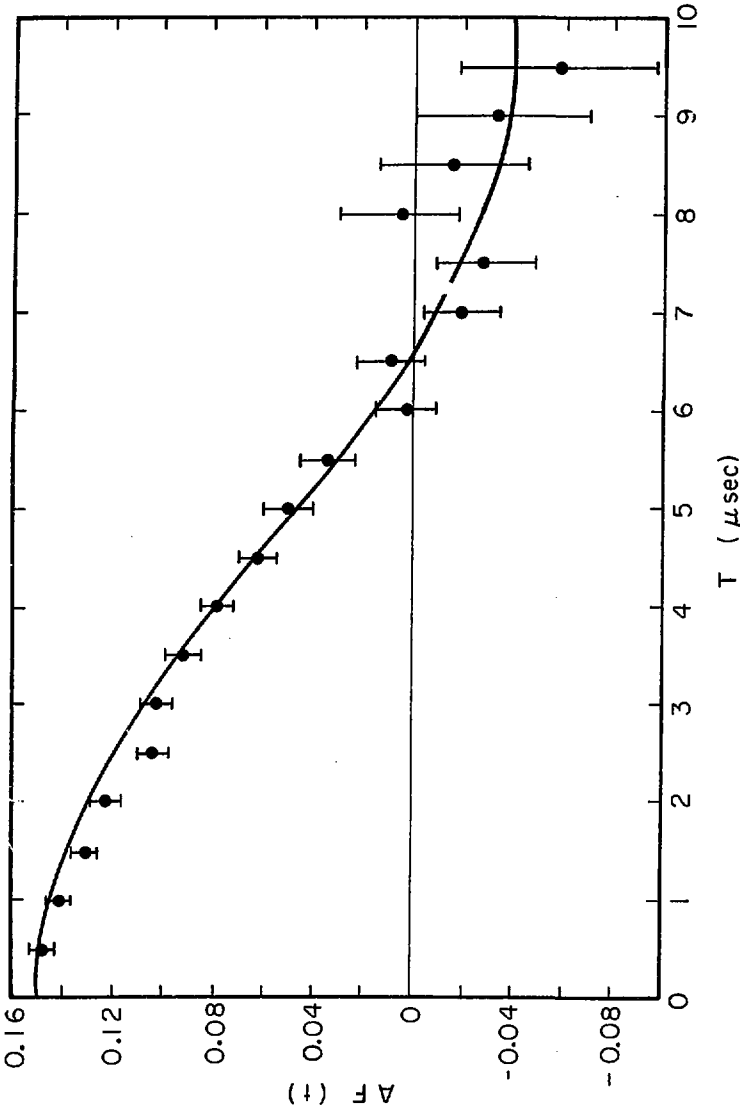
Fig. 11.
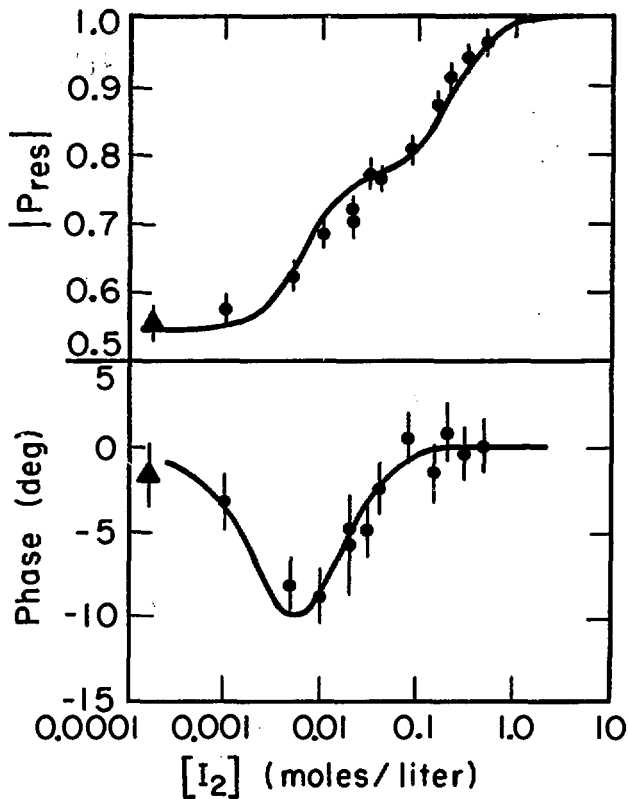
Fig. 12.   XBL734-2763

Fig. 13.

XBL 726-1086

BROMINE IN BENZENE AT 200 GAUSS

Fig. 14.

XBL 726-1104

Fig. 15.   XBL 7210-4166

NITRIC ACID IN WATER AT 100 GAUSS

XBL 726-1097

Fig. 16.

PERCHLORIC ACID IN WATER AT 4400 GAUSS

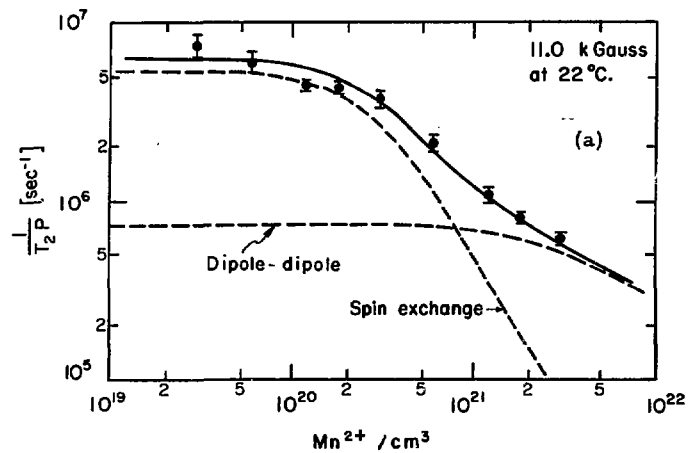LOG (CONC)
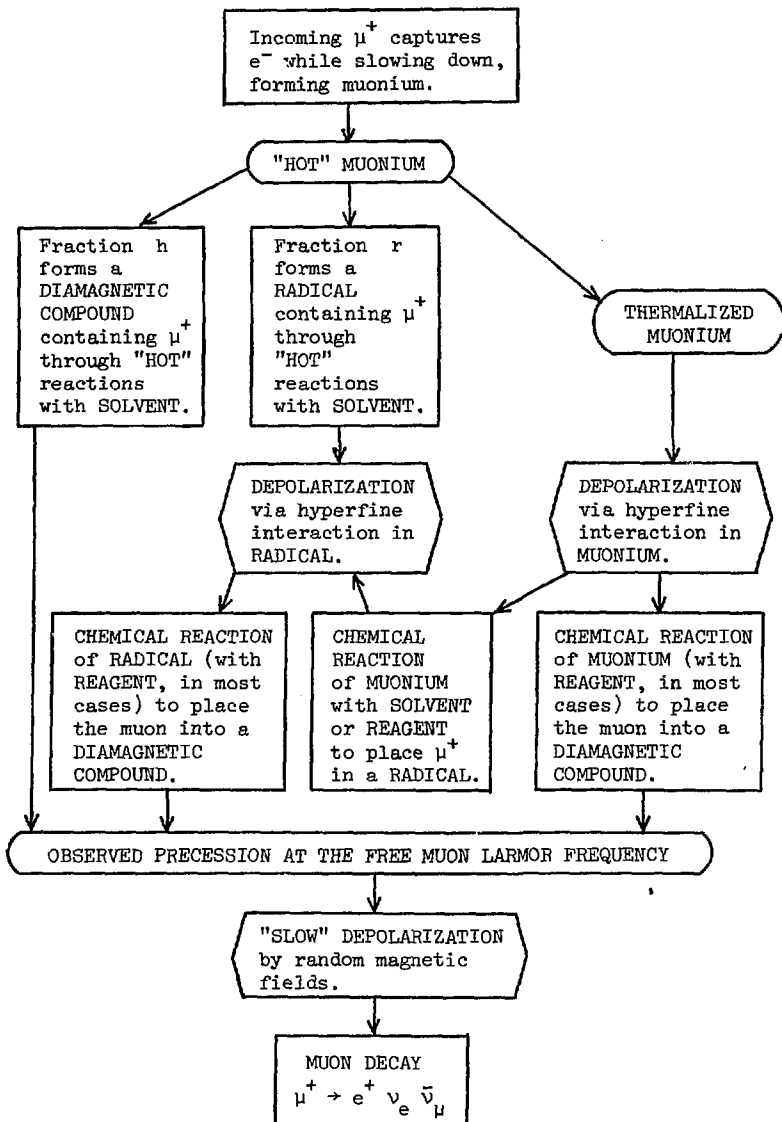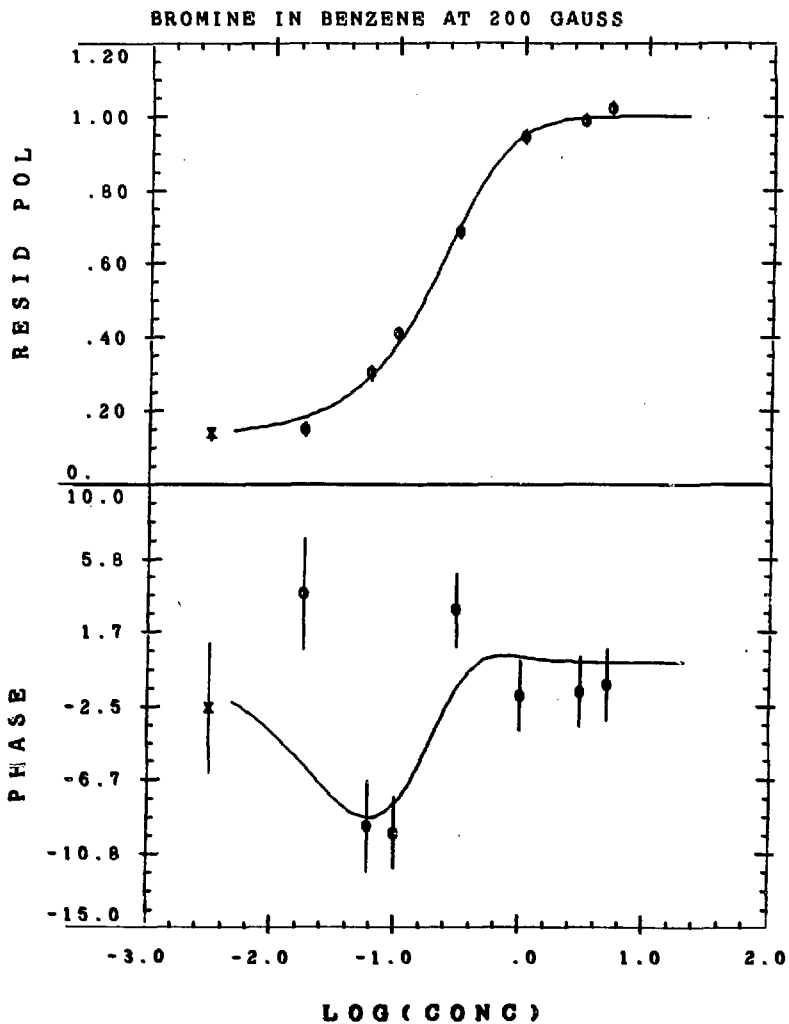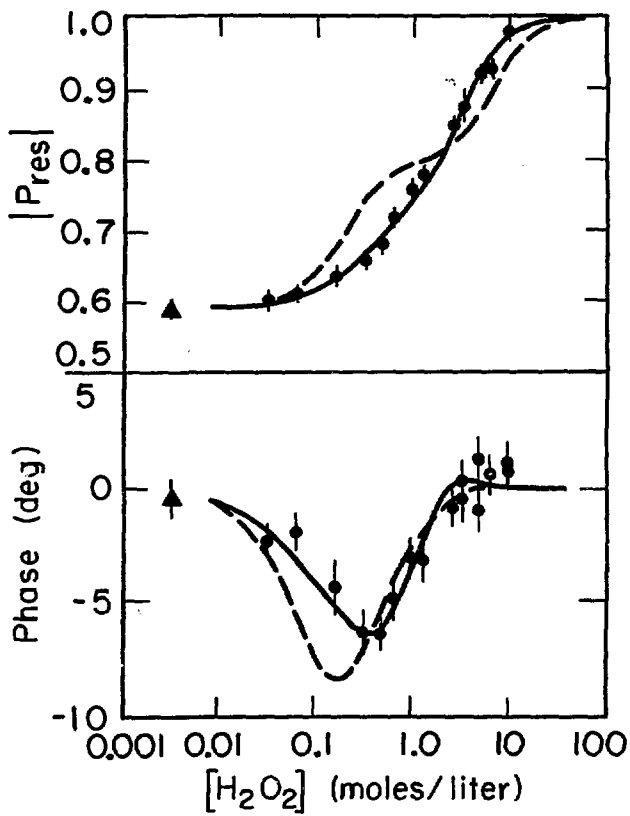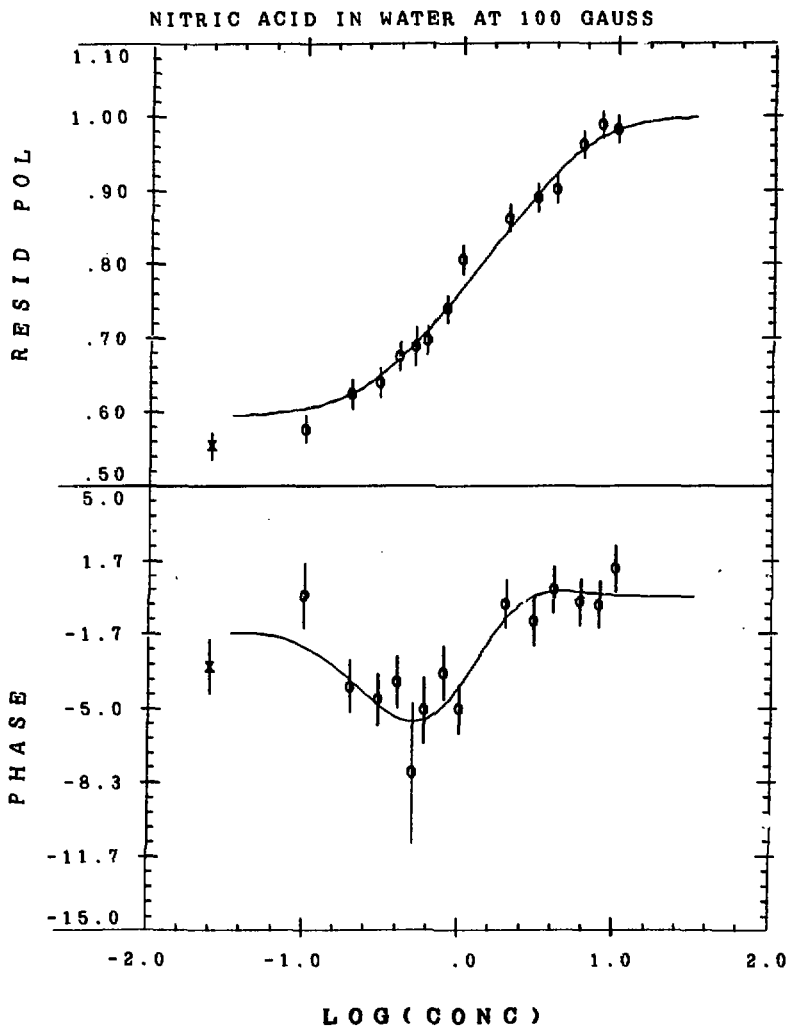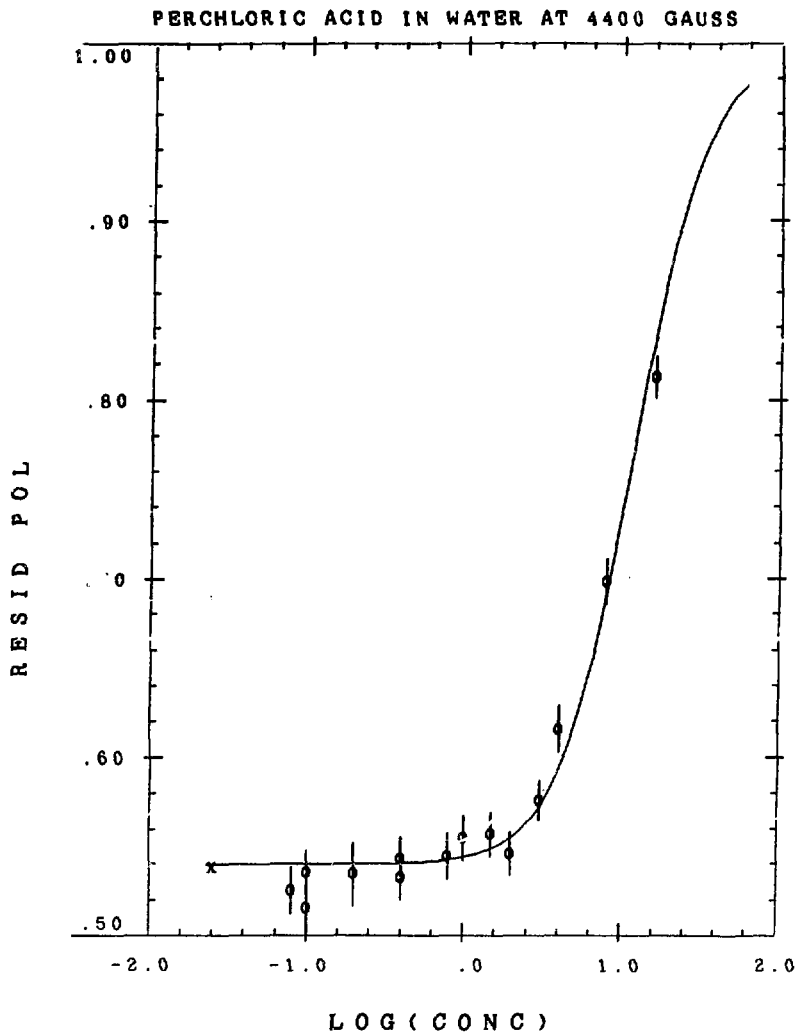
XBL 726-1098
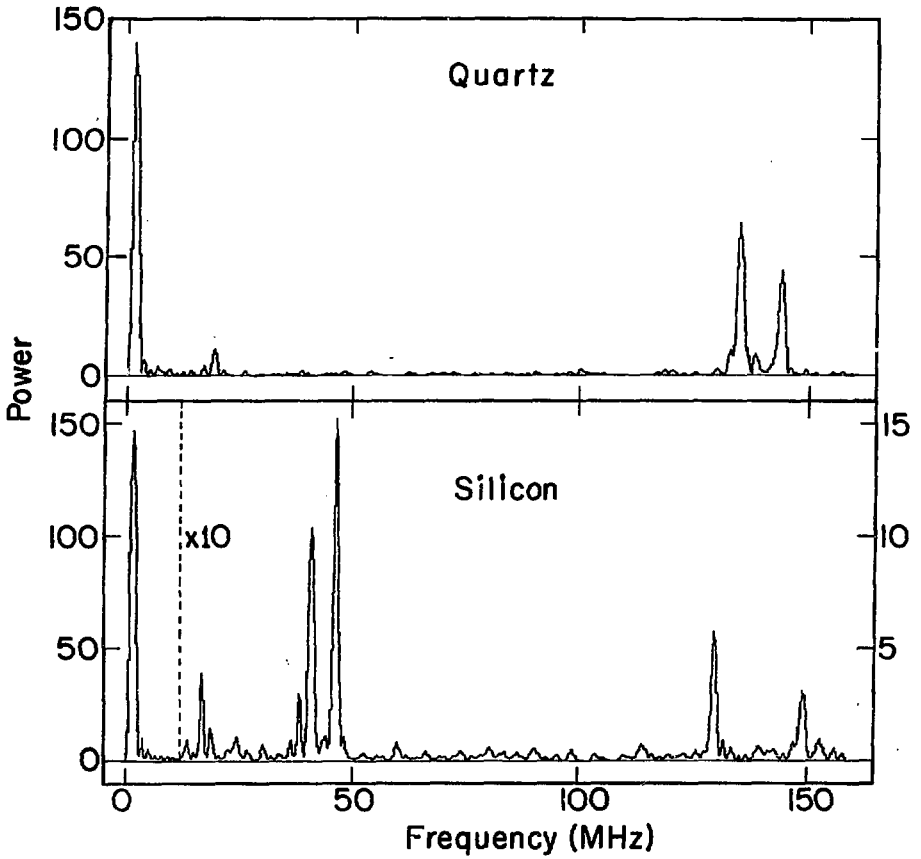
Fig. 17.
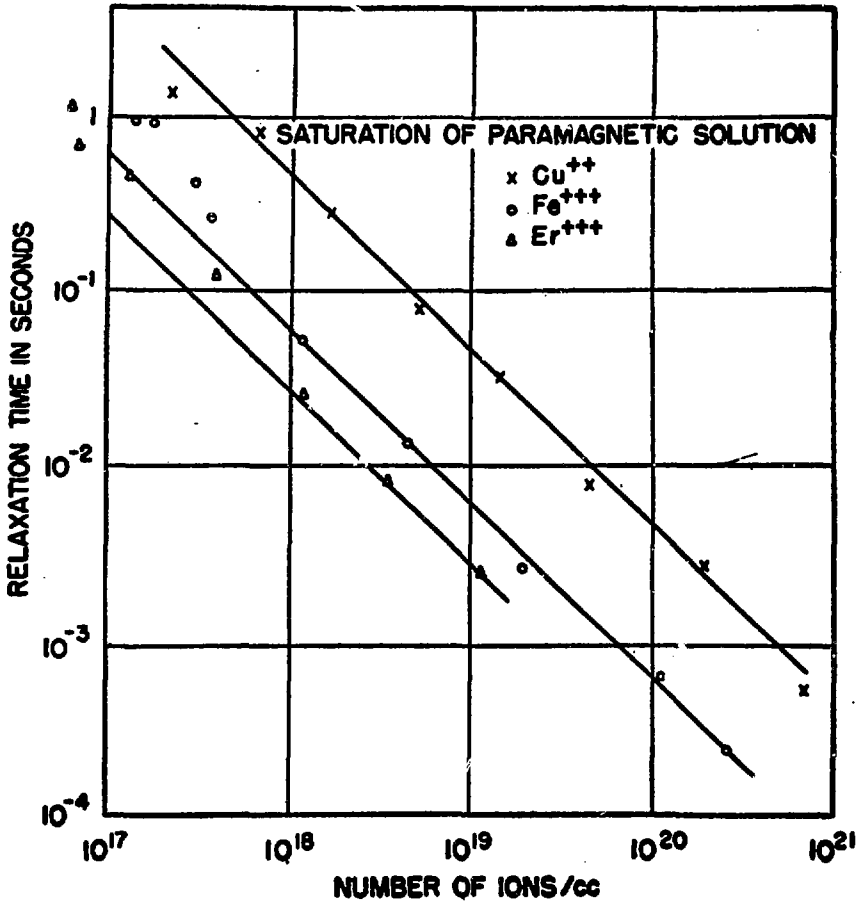
Fig. 18.

XBL 708-1702
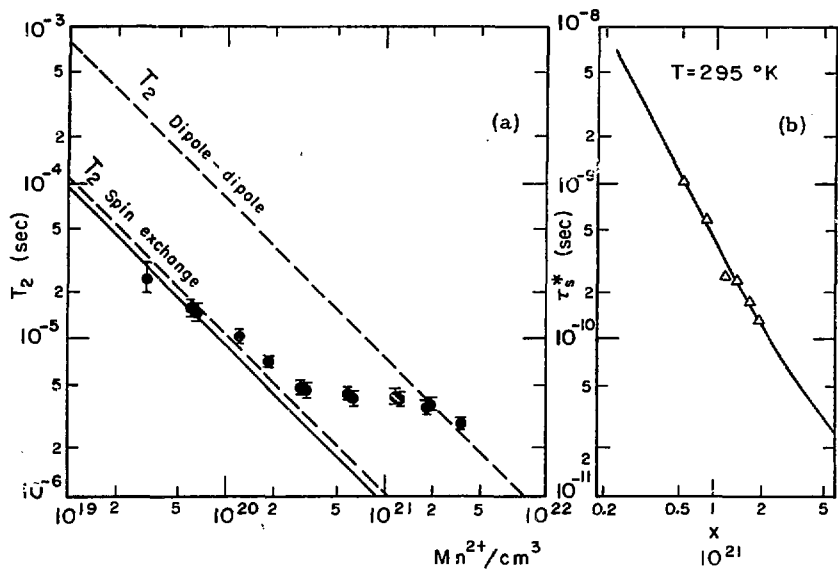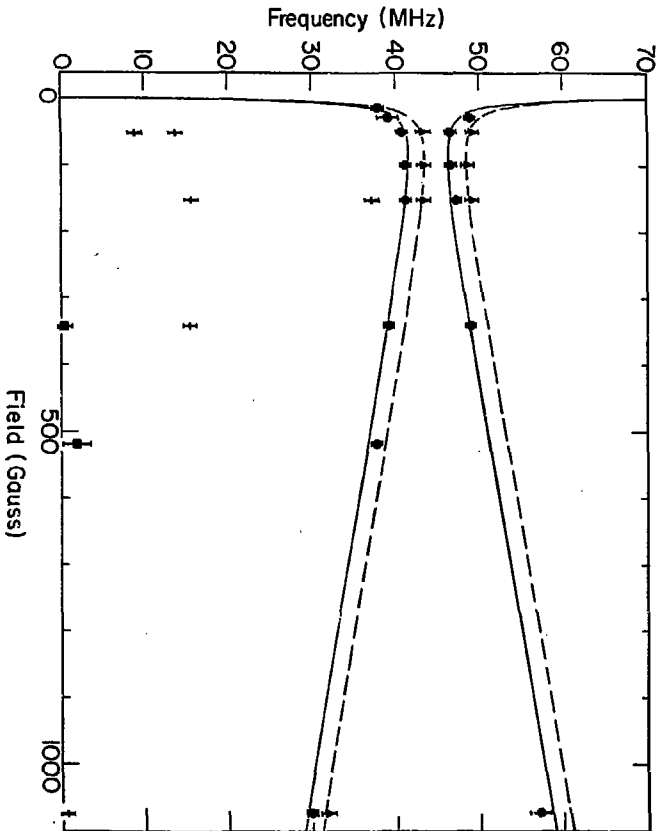
Fig. 19.

XBL718-4008
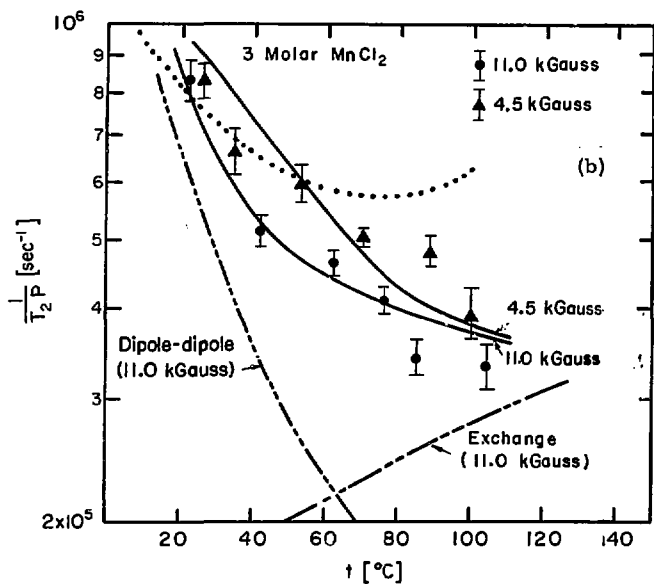
Fig. 20.   XBL718-4007

Fig. 21.   XBL734-2593

Fig. 22

XBL 734-2592